Enhanced Surface Reaction Kinetics and Charge Separation of p−n Heterojunction Co₃O₄/BiVO₄ Photoanodes

Xiaoxia Chang, Tuo Wang, Peng Zhang, Jijie Zhang, Ang Li, and Jinlong Gong*

Key Laboratory for Green Chemical Technology of Ministry of Education, School of Chemical Engineering and Technology, Tianjin University, Collaborative Innovation Center of Chemical Science and Engineering, Tianjin 300072, China

S *Supporting Information*

ABSTRACT: Surface reaction kinetics and bulk charge separation are both critical to the efficiency of solar water splitting. In addition to the well-documented surface catalytic effect, the promotion of bulk charge separation upon loading of cocatalysts has rarely been reported. This paper describes the synergetic enhancement of surface reaction kinetics and bulk charge separation by introducing discrete nanoisland p-type Co_3O_4 cocatalysts onto n-type $BiVO_4$, forming a p−n $Co_3O_4/BiVO_4$ heterojunction with an internal electric field to facilitate charge transport. Being highly dispersed on the surface of photoanodes, the nanoisland cocatalysts could suppress the formation of recombination centers at the photoanode/cocatalyst interface. This cocatalyst-loading method achieved a charge separation efficiency of up to 77% in the bulk and 47% on the surface of catalysts. An AM 1.5G photocurrent of 2.71 mA/cm² at 1.23 V versus the reversible hydrogen electrode for water oxidation was obtained, which is the highest photocurrent yet reported for Co-catalyzed undoped $BiVO_4$ photoanodes, with a photoconversion efficiency of 0.659%.

Photoelectrochemical (PEC) water splitting using sunlight has been widely regarded as one of the most promising routes for hydrogen production.[1−3] Recently, bismuth vanadate ($BiVO_4$) has emerged as a promising material for PEC water splitting, showing visible light photoactivity.[4] The monoclinic scheelite $BiVO_4$ with a band gap of ~2.4 eV exhibits a higher photocatalytic activity than its crystal-structure counterparts.[5] Its lower band-gap energy enables light absorption up to 11% of the solar spectrum compared to 4% for the conventional UV-sensitive TiO_2.[6] However, unmodified $BiVO_4$ photoanodes suffer from poor charge transport and sluggish water oxidation kinetics,[4] which limit its overall quantum efficiency. Therefore, various strategies such as doping with nitrogen[7] or molybdenum,[8,9] loading cocatalysts such as Co-Pi,[10] FeOOH, and NiOOH,[11] and construction of heterojunctions[12] have been employed to alleviate these restrictions.

Loading oxygen-evolution cocatalysts (OECs) has been shown as an effective approach to accelerate the surface reaction kinetics. Recently, Co-based OECs have drawn much attention because of their high efficiency under near-neutral pH conditions and the low cost of Co.[13] The transfer of photogenerated holes from the valence states of $BiVO_4$ to the $Co^{3+/2+}$ species during the water oxidation reaction greatly lowers the reaction overpotential.[4,14−16] Previously, Co-based catalysts have improved PEC water-splitting efficiency for various photoelectrodes including WO_3,[17] α-Fe_2O_3,[18,19] and ZnO, among others.[20] In addition, noticeable improvements were observed particularly for $BiVO_4$ photoanodes upon the loading of Co catalysts. Long et al. synthesized powdered composite of $BiVO_4/Co_3O_4$ on conductive substrates with fourfold improved incident photon-to-electron conversion efficiency (IPCE) compared to bare $BiVO_4$.[21] Zhong et al. obtained an AM 1.5G photocurrent of 1.4 mA/cm² at 1.23 V versus RHE (reversible hydrogen electrode) with Co-Pi catalyzed W-doped $BiVO_4$.[22] Lichterman et al. utilized $CoO_x/BiVO_4$ photoanodes to obtain a photocurrent of 1.49 mA/cm² at 1.23 V versus RHE under AM 1.5G.[23] Abdi et al. achieved the highest AM 1.5G photocurrent so far of 1.7 mA/cm² (at 1.23 V versus RHE) for Co-catalyzed undoped $BiVO_4$ photoanodes.[6] Wang et al. also showed 17-fold improved photocatalytic water-oxidation activity upon the addition of Co_3O_4 for $BiVO_4$.[16]

Although the surface catalytic effect of CoO_x has been well-recognized, the junction formed at the anode/OEC interface is also an important consideration. This anode/OEC junction may introduce more surface recombination centers that hamper the PEC performance and may also provide an additional driving force for the separation of charge carriers.[11] The introduction of interfacial recombination centers is especially a concern for continuous OECs layers deposited by electrodeposition, photo-assisted electrodeposition, or atomic layer deposition.[6,16,22−24] Kim et al. have investigated the interface states at the $BiVO_4$/OECs interface with increased charge recombination.[11] Zhong et al. also noticed the charge recombination at $CoO_x/BiVO_4$ interface and creatively deposited a continuous p-NiO thin film as the second OEC layer covering $CoO_x/BiVO_4$, which formed a p−n junction with the underlying n-$BiVO_4$ to enhance charge separation.[25]

Co_3O_4 is also a p-type semiconductor. With carefully controlled interfacial properties with the underlying n-type anode, p-Co_3O_4 is expected to form a p−n junction without depositing a second layer, while also acting as an effective OEC. This paper describes the loading of discrete p-Co_3O_4 nanoisland OECs to the n-$BiVO_4$ photoanodes, which enables simultaneous enhancement of surface reaction kinetics and bulk charge separation. First, we synthesized the $BiVO_4$ photoanodes with a nanoporous morphology to shorten the travel distance of photogenerated holes, reducing the chance of recombination.[11]

Second, the Co_3O_4 OECs have a p-type semiconducting nature and disperse on the surface of n-$BiVO_4$ to construct discontinuous p−n heterojunctions to enhance charge separation by an internal electric field. Lastly, the small particle size and high dispersion of Co_3O_4 may largely reduce the amount of recombination centers at the photoanode/OEC interface.[24,26−28] The resulting Co_3O_4/$BiVO_4$ electrode generated the highest AM 1.5G photocurrent for water oxidation among Co-catalyzed undoped $BiVO_4$-based photoanodes known to date. Considering that the loading amount would change the size of Co_3O_4 islands,[24] the effects of Co_3O_4 loading on PEC performance of the $BiVO_4$ photoanode are discussed in detail.

Nanoporous $BiVO_4$ photoanodes were synthesized by electrodeposition followed by annealing. The loading of Co_3O_4 OECs was carried out via drop-casting technique, and the mass of Co_3O_4 was adjusted by the drop volume of suspension liquid. (Experimental details are available in the Supporting Information.) To investigate the effects of Co_3O_4 loading on PEC performance of the $BiVO_4$ photoanode, we set the mass ratio of Co_3O_4/$BiVO_4$ to 2.0, 4.0, and 8.0 wt % (denoted as 2-Co/BV, 4-Co/BV, and 8-Co/BV, respectively). The particles within the white circles in the field-emission scanning electron microscopy (FESEM) image (Figure 1b) were confirmed by the energy-
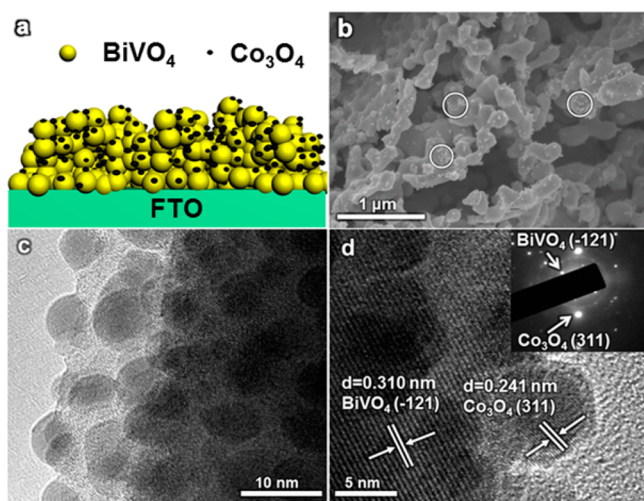

Figure 1. (a) Schematic of Co_3O_4/$BiVO_4$ photoanode. (b) FESEM. (c) TEM. and (d) HRTEM images of 4-Co/BV.

dispersive X-ray spectroscopy (EDX) to be Co_3O_4 (Figure S10a,b). The size of these discrete Co_3O_4 particles was ∼10 nm, as evidenced by TEM and high-resolution TEM (HRTEM) images of Co_3O_4 and 4-Co/BV (Figures S1c,d and 1c,d). X-ray diffraction (XRD) patterns (Figure S2) showed that $BiVO_4$ exhibits a monoclinic phase and pure Co_3O_4 exhibits a cubic phase. In addition, the loaded Co_3O_4 displays a lattice spacing of 0.241 nm (Figure 1d), corresponding to the (311) plane, and is well-dispersed according to Figure 1b. The high dispersion of Co_3O_4 is verified by XRD because no characteristic peak of Co_3O_4 was detected, even for 8-Co/BV (Figure S2b). Photoluminescence (PL) spectra (Figure S3) show that the major emission peak at about 507 nm is due to the electronic interband transition and is very close to the absorption edge of $BiVO_4$.[26] The PL intensity of 4-Co/BV was much weaker than that of $BiVO_4$, indicating that the direct recombination of photogenerated electron−hole pairs can be greatly suppressed upon the formation of Co_3O_4/$BiVO_4$ p−n heterojunction, and a more

efficient separation of photogenerated electron−hole pairs was obtained.[26,29]

PEC properties were all acquired with front-side illumination. To investigate the surface reaction kinetics of $BiVO_4$, 1 M sodium sulfite (Na_2SO_3) was added into the electrolyte as a hole scavenger in some cases (Figure 2b, d).[11,22] The typical current−
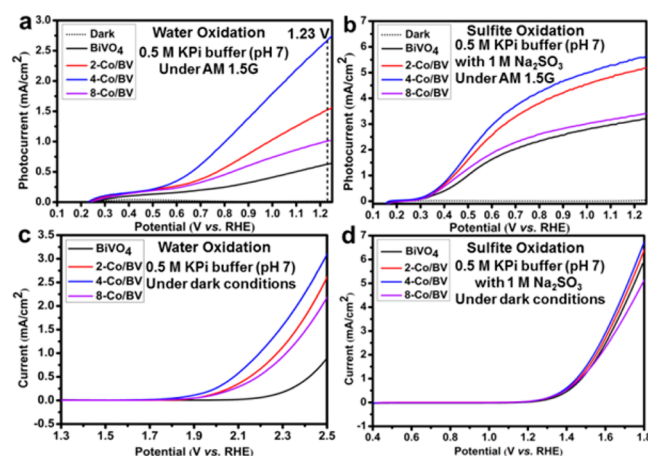
Figure 2. J−V curves of different photoanodes measured (a and b) with and (c and d) without AM 1.5G illumination (100 mW/cm²) for (a and c) water oxidation (without 1 M Na_2SO_3) and (b and d) sulfite oxidation (with 1 M Na_2SO_3). Photoactivity of different samples (panel b) with equally fast sulfite oxidation kinetics reveals the charge separation effect of Co_3O_4.

potential (J−V) curves of water oxidation and sulfite oxidation with/without AM 1.5G are shown in Figure 2. The significant improvement of photocurrents in Figure 2a,b clearly reveals the enhanced PEC activity upon loading of Co_3O_4. An AM 1.5G photocurrent of 2.71 mA/cm² at 1.23 V versus RHE for water oxidation was achieved with 4-Co/BV. Because of the poor water oxidation kinetics of $BiVO_4$, the photogenerated holes accumulated on the surface of photoanodes, resulting in serious surface charge recombination,[22] as evidenced by the great difference of the two black curves in Figure 2a,b for bare $BiVO_4$ as well as the large photocurrent transients with switching illumination (Figure S4a, black curve). Our results indicate that loading of Co_3O_4 significantly reduces the amount of holes accumulated and thus prohibits the surface recombination during water oxidation, as evidenced by the much less pronounced photocurrent transients (Figure S4a, blue curve).

The dark J−V curve of 4-Co/BV for water oxidation shows a noticeable cathodic shift (∼420 mV) of onset potential compared to the curve of pure $BiVO_4$, indicating the catalytic effect of Co_3O_4 OECs (Figure 2c). However, no obvious shift was observed between Co_3O_4-loaded and pure $BiVO_4$ samples for sulfite oxidation under dark conditions (Figure 2d), suggesting equally fast sulfite oxidation kinetics on the surface of $BiVO_4$ and Co_3O_4. The Na_2SO_3 hole scavenger also erased the surface recombination of $BiVO_4$ because the photocurrent spikes of $BiVO_4$ were not observed (Figure S4b, red curve). Because the surface catalytic and passivation effects of Co_3O_4 are both ruled out, the significant improvement of photocatalytic sulfite oxidation performance upon loading of Co_3O_4 (Figure 2b) clearly indicates a charge-separation effect in the bulk.

It should be noted that the formation of p−n Co_3O_4/$BiVO_4$ junction can greatly enhance the charge separation owing to the internal electric field, which outperforms the negative effect of

electrical resistance of Co_3O_4 and recombination centers at Co_3O_4/$BiVO_4$ interface. The synergetic enhancement of charge separation by p−n Co_3O_4/$BiVO_4$ junction and improved surface reaction kinetics with Co_3O_4 OECs resulted in a great improvement in photocurrent for water oxidation. Decreased photocatalytic performance for sulfite oxidation was reported for $BiVO_4$ upon loading of NiOOH/FeOOH, probably because of the lack of optimized p−n junctions or the introduction of excessive interfacial defects.[11]

UV−vis absorptance spectra (Figure S5) show that the absorption edge of pure $BiVO_4$ and Co_3O_4 was 504 and 599 nm, respectively, corresponding to the direct band gap energy (E_g) of 2.46 and 2.07 eV, respectively, in accordance with the reported values.[16,21,31] Even though Co_3O_4 may compete with the underlying photoanode for light absorption,[32] the photo-excitation of p-type Co_3O_4 is necessary to obtain the additional driving force for charge separation at the p−n junction. The band positions of pure $BiVO_4$ and Co_3O_4 were predicted theoretically from the absolute electronegativity and corrected for the deviation from the point of zero charge to pH 7 (details in the Supporting Information).[16,31] According to the estimated conduction, valence band edges, and E_g values of $BiVO_4$ and Co_3O_4 (Table S1), we propose a mechanism of charge separation for p-Co_3O_4/n-$BiVO_4$ heterojunction (Scheme 1). The photo-

Scheme 1. Band Diagram and Mechanism of Charge Separation for p-Co_3O_4/n-$BiVO_4$ Heterojunction
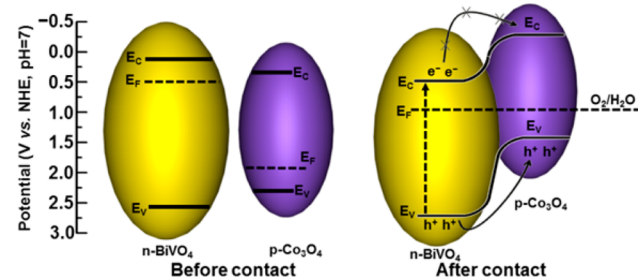
electrons from $BiVO_4$ are prohibited from migrating to Co_3O_4, whereas the photogenerated holes on the valence band of $BiVO_4$ can travel to that of Co_3O_4.[31] Furthermore, the highly dispersed state of Co_3O_4 could suppress the formation of interfacial recombination centers. As a consequence, the separation of photogenerated electron−hole pairs is significantly improved. In addition, the sluggish surface reaction kinetics is overcome by the Co_3O_4 OECs, which further lowers the overpotential for water oxidation.[15,16]

To quantify the contributions of discrete p-type Co_3O_4 nanoislands to the enhancement of charge separation and surface reaction kinetics, the efficiency of charge transport in the bulk (η_{bulk}, relating to bulk charge separation) and surface charge transfer ($\eta_{surface}$, relating to surface charge separation, i.e., surface reaction kinetics) were determined independently and are displayed in Figure 3 (details in the Supporting Information). The results show that with a loading amount of 4.0 wt %, $\eta_{surface}$ reached 47% at 1.23 V versus RHE, which was increased threefold compared to that of pure $BiVO_4$ (16%). η_{bulk} was also improved from 56% for pure $BiVO_4$ to 77% for 4-Co/BV at 1.23 V versus RHE, exhibiting a great advantage of this cocatalyst-loading method compared to other works (Figure 3, black and blue curves).[8,10,30]

The IPCE measured at 1.23 V versus RHE of 4-Co/BV is ∼4 times that of pure $BiVO_4$, reaching up to 50% at 460 nm and
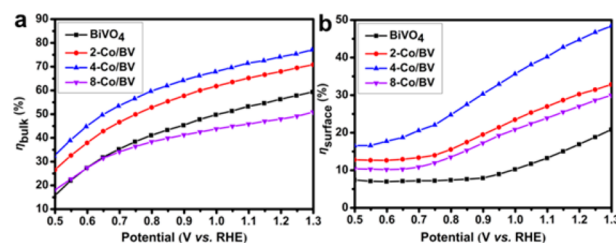
Figure 3. Charge separation efficiency (a) in the bulk (η_{bulk}) and (b) on the surface ($\eta_{surface}$) of photoanodes.

varying between 45−50% at 460−360 nm (Figure S6). In addition, photocurrent density of ∼0.71 mA/cm^2 for $BiVO_4$ and ∼2.54 mA/cm^2 for 4-Co/BV can be estimated by integrating the IPCE over the AM 1.5G solar spectrum (Figure S7). The estimated values are very close to the measured ones of 0.67 and 2.71 mA/cm^2 for $BiVO_4$ and 4-Co/BV in the J−V curves, respectively.[33] Furthermore, an improved photoconversion efficiency (PCE) of 0.659% at 0.83 V versus RHE was obtained with 4-Co/BV, fourfold that of pure $BiVO_4$ (Figure S8).

Moreover, with increasing Co_3O_4 loading, the photocurrent density initially increased, and the 4-Co/BV sample exhibited the highest value. However, the photocurrent decreased sharply for 8-Co/BV with or without the presence of Na_2SO_3 (Figure 2a,b). From FESEM and HRTEM images, the Co_3O_4 nanoparticles with an initial size of ∼10 nm tended to aggregate into larger particle clusters for 8-Co/BV (white circles in Figures S9a,b,c and 1c) where the clusters were confirmed to be Co_3O_4 by EDX (Figure S10d). Normally, cocatalysts with smaller size and higher dispersion exhibit higher catalytic activity because of the larger surface area with abundant active sites, which has been widely proved.[24,27,28] Similarly, the decrease of surface area and loss of active sites of 8-Co/BV likely lead to the reaction kinetics being slower than those of 4-Co/BV. In addition, the onset potentials of dark J−V curves in Figure 2c also indicate a decrease of electrocatalytic activity of 8-Co/BV compared to 4-Co/BV. Meanwhile, η_{bulk} of 8-Co/BV is the lowest (Figure 3a).

The above findings indicate that larger particle clusters of Co_3O_4 may exhibit more interfacial defects and larger resistance for the charge to transport through, as demonstrated by electrochemical impedance spectroscopy (EIS) in Figure 4.
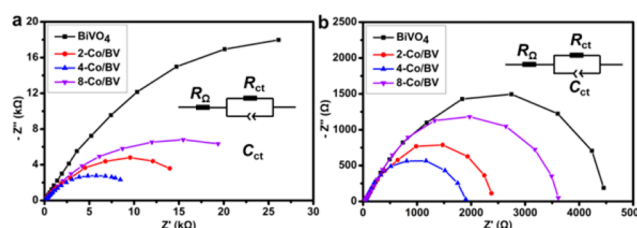
Figure 4. EIS spectra of photoanodes measured under the open-circle potential and AM 1.5G (100 mW/cm^2) in KPi buffer solution (pH 7) (a) without and (b) with 1 M Na_2SO_3.

The EIS results show that only one semicircle was observed for each sample and thus can be fitted with the Randles equivalent circuit model (inset of Figure 4).[34] In this model, the element R_Ω is the resistance relating to charge transport, which contains the resistance of semiconductor catalysts, SnO_2 layer of FTO substrates, the electrolyte, and wire connections in the whole circuit. The elements of R_{ct} and C_{ct} are related to the charge transfer at the interface of the photoelectrode/electrolyte. A

smaller semidiameter of the semicircle represents a better charge-transfer ability (i.e., faster surface reaction kinetics).[34] As shown in Figure 4, 4-Co/BV exhibited the smallest semidiameter in both electrolytes, which was in agreement with its higher PEC activity. Meanwhile, 8-Co/BV exhibited a worse charge-transfer ability than 4-Co/BV probably because of the agglomeration of Co_3O_4 nanoislands. The fitting results of R_Ω with low uncertainty for each sample (Table S2) reveal further insights into the effects of Co_3O_4 loading on the bulk charge transport. 8-Co/BV exhibited the highest R_Ω resulting from the increase of the catalysts resistance especially when all EIS data were collected under the same conditions with Co_3O_4 loading as the only variable. Therefore, the charge separation efficiency of 8-Co/BV decreased significantly both on the surface (i.e., surface reaction kinetics) and in the bulk, leading to a lower PEC activity than that of 4-Co/BV. This also indicates the significance of highly dispersed state of the loaded Co_3O_4.

We have demonstrated that the p-Co_3O_4/n-$BiVO_4$ heterojunction with discrete Co_3O_4 nanoisland OECs can effectively enhance the surface reaction kinetics and charge separation of the $BiVO_4$ photoanodes simultaneously, owing to the synergistic effects of OECs and p−n heterojunction. The highly dispersed state of Co_3O_4 plays an important role in suppressing the excessive formation of recombination centers at Co_3O_4/$BiVO_4$ interface as well as improving the surface reaction kinetics. An AM 1.5G photocurrent of 2.71 mA/cm^2 at 1.23 V versus RHE for water oxidation was achieved, which is the highest photocurrent yet reported for Co-catalyzed undoped $BiVO_4$ photoanodes. An improved PCE of 0.659% at 0.83 V versus RHE was also obtained. Quantitative analysis indicates that the bulk and surface recombination of charge carriers were both greatly suppressed upon loading of p-Co_3O_4. A higher Co_3O_4 loading of 8.0 wt % led to a reduced PEC performance because of the agglomeration of Co_3O_4 particles, leading to hampered surface reaction kinetics and bulk charge separation. Our work could provide insights into the rational design of the photocatalysts/OECs structure. In addition to faster surface reaction kinetics, properly designed cocatalysts can achieve higher charge-separation efficiency in the bulk, which is an efficient way to further enhance the PEC activity.

■ ASSOCIATED CONTENT

Ⓢ Supporting Information

Experimental details and supporting data. The Supporting Information is available free of charge on the ACS Publications website at DOI: 10.1021/jacs.5b04186.

■ AUTHOR INFORMATION

Corresponding Author
*jlgong@tju.edu.cn

Author Contributions
X.C. and T.W. contributed equally to the creation of this work.

Notes
The authors declare no competing financial interest.

■ ACKNOWLEDGMENTS

■ REFERENCES

(1) Wang, T.; Luo, Z.; Li, C.; Gong, J. *Chem. Soc. Rev.* **2014**, *43*, 7469.
(2) Osterloh, F. E. *Chem. Soc. Rev.* **2013**, *42*, 2294.
(3) Fujishima, A.; Honda, K. *Nature* **1972**, *238*, 37.
(4) Park, Y.; McDonald, K. J.; Choi, K. S. *Chem. Soc. Rev.* **2013**, *42*, 2321.
(5) Tokunaga, S.; Kato, H.; Kudo, A. *Chem. Mater.* **2001**, *13*, 4624.
(6) Abdi, F. F.; van de Krol, R. *J. Phys. Chem. C* **2012**, *116*, 9398.
(7) Tan, G.; Zhang, L.; Ren, H.; Huang, J.; Yang, W.; Xia, A. *Ceram. Int.* **2014**, *40*, 9541.
(8) Seabold, J. A.; Zhu, K.; Neale, N. R. *Phys. Chem. Chem. Phys.* **2014**, *16*, 1121.
(9) Parmar, K. P.; Kang, H. J.; Bist, A.; Dua, P.; Jang, J. S.; Lee, J. S. *ChemSusChem* **2012**, *S*, 1926.
(10) Zhou, M.; Bao, J.; Bi, W.; Zeng, Y.; Zhu, R.; Tao, M.; Xie, Y. *ChemSusChem* **2012**, *S*, 1420.
(11) Kim, T. W.; Choi, K. S. *Science* **2014**, *343*, 990.
(12) Saito, R.; Miseki, Y.; Sayama, K. *Chem. Commun.* **2012**, *48*, 3833.
(13) Kanan, M. W.; Nocera, D. G. *Science* **2008**, *321*, 1072.
(14) Risch, M.; Khare, V.; Zaharieva, I.; Gerencser, L.; Chernev, P.; Dau, H. *J. Am. Chem. Soc.* **2009**, *131*, 6936.
(15) McAlpin, J. G.; Surendranath, Y.; Dinca, M.; Stich, T. A.; Stoian, S. A.; Casey, W. H.; Nocera, D. G.; Britt, R. D. *J. Am. Chem. Soc.* **2010**, *132*, 6882.
(16) Wang, J. R.; Osterloh, F. E. *J. Mater. Chem. A* **2014**, *2*, 9405.
(17) Seabold, J. A.; Choi, K.-S. *Chem. Mater.* **2011**, *23*, 1105.
(18) Zhong, D. K.; Sun, J.; Inumaru, H.; Gamelin, D. R. *J. Am. Chem. Soc.* **2009**, *131*, 6086.
(19) Zhong, D. K.; Cornuz, M.; Sivula, K.; Grätzel, M.; Gamelin, D. R. *Energy Environ. Sci.* **2011**, *4*, 1759.
(20) Steinmiller, E. M.; Choi, K. S. *Proc. Natl. Acad. Sci. U.S.A.* **2009**, *106*, 20633.
(21) Long, M. C.; Cai, W. M.; Kisch, H. *J. Phys. Chem. C* **2008**, *112*, 548.
(22) Zhong, D. K.; Choi, S.; Gamelin, D. R. *J. Am. Chem. Soc.* **2011**, *133*, 18370.
(23) Lichterman, M. F.; Shaner, M. R.; Handler, S. G.; Brunschwig, B. S.; Gray, H. B.; Lewis, N. S.; Spurgeon, J. M. *J. Phys. Chem. Lett.* **2013**, *4*, 4188.
(24) Ran, J.; Zhang, J.; Yu, J.; Jaroniec, M.; Qiao, S. Z. *Chem. Soc. Rev.* **2014**, *43*, 7787.
(25) Zhong, M.; Hisatomi, T.; Kuang, Y.; Zhao, J.; Liu, M.; Iwase, A.; Jia, Q. M.; Nishiyama, H.; Minegishi, T.; Nakabayashi, M.; Shibata, N.; Niishiro, R.; Katayama, C.; Shibano, H.; Katayama, M.; Kudo, A.; Yamada, T.; Domen, K. *J. Am. Chem. Soc.* **2015**, *137*, 5053.
(26) Yu, J.; Ran, J. *Energy Environ. Sci.* **2011**, *4*, 1364.
(27) Kato, H.; Asakura, K.; Kudo, A. *J. Am. Chem. Soc.* **2003**, *125*, 3082.
(28) Chen, X.; Wu, G.; Chen, J.; Chen, X.; Xie, Z.; Wang, X. *J. Am. Chem. Soc.* **2011**, *133*, 3693.
(29) Zhang, J.; Zhang, M.; Sun, R.; Wang, X. *Angew. Chem., Int. Ed.* **2012**, *S1*, 10145.
(30) Seabold, J. A.; Choi, K. S. *J. Am. Chem. Soc.* **2012**, *134*, 2186.
(31) Long, M.; Cai, W.; Cai, J.; Zhou, B.; Chai, X.; Wu, Y. *J. Phys. Chem. B* **2006**, *110*, 20211.
(32) Trotochaud, L.; Mills, T. J.; Boettcher, S. W. *J. Phys. Chem. Lett.* **2013**, *4*, 931.
(33) Li, Y.; Zhang, L.; Torres-Pardo, A.; Gonzalez-Calbet, J. M.; Ma, Y.; Oleynikov, P.; Terasaki, O.; Asahina, S.; Shima, M.; Cha, D.; Zhao, L.; Takanabe, K.; Kubota, J.; Domen, K. *Nat. Commun.* **2013**, *4*, 2566.
(34) Klahr, B.; Gimenez, S.; Fabregat-Santiago, F.; Hamann, T.; Bisquert, J. *J. Am. Chem. Soc.* **2012**, *134*, 4294.